Chemical Engineering Journal 519 (2025) 165392

Contents lists available at ScienceDirect

Chemical Engineering Journal

journal homepage: www.elsevier.com/locate/cej

4D printed kirigami metamaterial with reconfigurability for dual-mode displacement-pressure sensing

Song Liu [a], Zhaoxuan Niu [b], Wei Zhao [c,*], Chengjun Zeng [c], Yanju Liu [c,d], Jinsong Leng [a,*]

[a] Centre for Composite Materials and Structures, Harbin Institute of Technology (HIT), No. 2 Yikuang Street, P.O. Box 3011, Harbin 150080, People's Republic of China
[b] School of Chemistry and Chemical Engineering, Harbin Institute of Technology (HIT), Harbin 150001, People's Republic of China
[c] Department of Astronautical Science and Mechanics, Harbin Institute of Technology (HIT), P.O. Box 301, No. 92 West Dazhi Street, Harbin 150001, People's Republic of China
[d] Suzhou Research Institute, Harbin Institute of Technology(HIT), Suzhou 215100, People's Republic of China

ARTICLE INFO

Keywords:
Kirigami metamaterial
Reconfigurable
Dual-mode sensor
4D Printing
Triboelectric-piezoelectric

ABSTRACT

Mechanical metamaterials have been widely investigated because of their unique mechanical properties. Due to their exceptional properties, mechanical metamaterials can be combined with other materials and technologies to integrate more functions, such as applications in sensor design. The low stiffness, negative stiffness and high sensitivity of Kirigami mechanical metamaterials contribute to improving the sensing accuracy and efficiency of the sensor. This work proposes a sensor based on a 4D printed pyramid Kirigami mechanical metamaterials (PKMM). And we integrates composite triboelectric and piezoelectric sensing mechanisms for comprehensive monitoring of multi-dimensional mechanical signals. This sensor shows surface conformality and reconfigurability, allowing for adaptable shape morphing across different environments. The composite triboelectric-piezoelectric mechanism enables the sensor to exhibit high sensitivity, broadening the pressure sensing range and facilitating precise measurement of displacement variables. This PKMM-based sensor effectively monitors the conformal motion of the human elbow joint. And its axial array configuration allows for the sensing of complex multi-dimensional deformations. Moreover, the modular island-bridge array can accurately analyze multi-point load distributions. This work highlights the PKMM's applications in biological motion monitoring and intelligent protective equipment, providing innovative solutions for multifunctional flexible sensors.

1. Introduction

Mechanical metamaterials have been widely investigated in recent years because of their special mechanical properties. These unique properties surpass the performance limitations of conventional materials, which are enabled by precisely engineered structures [1–5]. Kirigami mechanical metamaterials break the continuity constraint by utilizing trimming or cutting, significantly improving the kinematic freedom of the structure. As a result, it has unique stretchability and exhibits unprecedented conformability [6–11]. Kirigami mechanical metamaterials are also widely used in fields such as wearable devices and flexible electronic sensors. Modern flexible electronic sensing technologies rely on four core operating mechanisms: piezoresistive, capacitive, piezoelectric and triboelectric [12–14]. Among them, piezoelectric and triboelectric technologies have attracted much attention due to their unique self-powered characteristics [15–17]. These devices have the capacity to directly and efficiently convert mechanical energy from the environment into electrical energy, thereby powering micro-electronic devices [18]. Triboelectric nanogenerator (TENG) has been rapidly progressing in research due to its relatively simple preparation process and flexibility in material selection [19–22]. TENGs utilize two primary operational modes: contact-separation mode and sliding mode [23–25]. These modes deliver high low-frequency energy conversion efficiency with cost-effective manufacturing, enabling widespread deployment in distributed energy systems [26]. However, the charge generation of TENG originates from the transient of material contact-separation or sliding, and its output signal has a natural time discontinuity. It is generated only at the instant of interfacial separation of the friction layer material, with high signal intensity but extremely short duration. And there is a time interval between neighbouring pulses that is obviously limited by the cycle of mechanical motion, resulting in the output of a large number of blank signals [27–29]. This discrete

* Corresponding authors.
E-mail addresses: zhaowei_2022@163.com (W. Zhao), lengjs@hit.edu.cn (J. Leng).

https://doi.org/10.1016/j.cej.2025.165392
Received 10 April 2025; Received in revised form 18 June 2025; Accepted 26 June 2025
Available online 2 July 2025

pulse characteristic makes it sensitive to sudden movements (e.g., impacts) but difficult to capture sustained static pressure. Flexible piezoelectric sensors, on the other hand, can respond to continuous deformation with charge output synchronised with mechanical strain. Flexible piezoelectric sensors maintain persistent electrical output under static pressure, bridging the temporal gap between intermittent TENG output pulses.

It is evident that Kirigami mechanical metamaterials have demonstrated considerable potential for application in the domain of wearable devices and flexible electronics. The primary reason for this is their distinctive programmable deformation capability and exceptional mechanical properties. Moreover, the diverse deformation characteristics of Kirigami mechanical metamaterials are profoundly related to the core mechanisms of the sensing functions of these devices. However, most of the species in Kirigami-based sensors act as strain sensors by virtue of their tensile properties in combination with piezoresistive materials. There are numerous additional types and properties of Kirigami mechanical metamaterials that have yet to be developed for utilisation in the domain of wearable devices. Such absence limits the upper performance limit and innovative potential of Kirigami mechanical metamaterials for advanced sensing applications. A notable research gap pertains to the application of combined TENG and piezoelectric sensing systems. Because most of the Kirigami mechanical metamaterials lack the physical environment for TENG contact-separation, only a few studies have explored this aspect [30]. Instead, we note a class of pyramid Kirigami mechanical metamaterials (PKMM) that are different from the most common ribbon or square-cutting Kirigami. The deformation of PKMM is mainly stretching and unfolding in the *Z*-axis direction, which has the advantage of being arbitrarily reconfigurable between 2D and 3D [31–34]. It is noteworthy that the reconfiguration of PKMM instigates dynamic contact separation events between its central region and the substrate. This kinematic behaviour intrinsically satisfies the operational requirements of TENG. The integration of TENG into PKMM is considered to be a methodology for the design of reconfigurable multifunctional sensors. In addition, PKMM exhibits properties such as low stiffness, zero stiffness or even negative stiffness during reconfiguration. These properties enable it to generate significant deformation responses under small external forces and achieve highly sensitive sensing of mechanical stimuli or deformation [35,36]. High sensitivity sensing of deformation can be achieved by integrating flexible piezoelectric sensors on the PKMM structure.

Furthermore, the PKMM's configurability presents a distinctive opportunity to address this research gap. Combining PKMM with shape memory polymers (SMPs) can achieve intelligent regulation of sensing function and structural morphology. SMPs represent smart materials capable of switching between temporary and permanent configurations [37,38]. This property facilitates the development of reconfigurable multifunctional sensors. SMPs exhibit stimulus-responsive recovery to their memorised configuration under thermal, magnetic, electric, photonic, or chemical stimuli. Such an intrinsic property is termed the shape memory effect (SME). 4D printed extends 3D fabrication by enabling direct manufacturing of stimuli-responsive structures. This process utilizes smart materials as functional consumables. Using 4D printed, SMP-based PKMM sensors can be programmed with temporary shapes and reconfigured between upright unfolded and planar states in response to external stimuli.

This work presents a PKMM-based smart sensor through 4D printed, utilizing a composite triboelectric-piezoelectric mechanism. The integrated system demonstrates hypersensitivity, stability, and reconfigurability. The sensor structure exhibits the properties of low and negative stiffness. Its unique deformation mode allows for dual-variable and multi-segment perception of both displacement and pressure, leveraging triboelectric and piezoelectric technologies. Moreover, the application of 4D printed technology imparts reconfigurable capabilities to the sensor. This function enables PKMM sensors to modify their morphology and adapt their functions based on external environmental conditions, allowing for enhanced versatility in various scenarios.

2. Results and discussion

2.1. Design of the PKMM

The design of classical pyramid Kirigami is characterised by two primary variables: the number of layers and the number of sides [31,39]. The two-layer, four-sided pyramid Kirigami is utilised as the primary research platform for this work due to operational constraints in practical implementation. Firstly, it is evident that an augmentation in the structural layers of the platform results in a substantial diminution of its effective contact area. This area reduction compromises the platform's primary function as a carrier substrate for TENGs and piezoelectric materials. Secondly, it is important to note that an excess of sides would render the experiment unwieldy. The system is susceptible to elevated error, owing to the superfluous piezoelectric sensing for strains. The lower three-sided pyramid Kirigami demonstrates a clear deficiency in experimental data volume. Consequently, the design of this work is centred on the design study of a two-layer four-sided PKMM. As illustrated in Fig. 1, there are two distinct states of the PKMM structure: the planar state (Fig. 1a) and the 3D state (Figs. 1 cd). The PKMM structure is composed of three principal components: the Hub, the Tab and the Ligament (Fig. 1b). The Hub functions as the connection node, thereby establishing the hierarchical structure among the components. The function of the Tab is to facilitate the connection between the Ligament and the Hub, thereby enabling the transfer of load. The Ligament facilitates the rotation and upright deformation of the entire structure through the processes of buckling and torsion. As the structure transitions from the planar state to the 3D state, a combined Platform and Link arm can be introduced to provide support for the sensors (Fig. 1d).

Upon observation of the classical pyramid Kirigami, it is evident that the function of the Hub is solely to facilitate connection to the Ligament. The width of the Tab is reduced, while the width of the Ligament is increased. This modification is intended to enhance the effective area of the PKMM sensors. The individual geometric variables of the PKMM are displayed in Figs. 1ab (Specific parameters in Table S1, Supporting Note S1). In the design scheme under consideration, the Hub width t has been fixed and reduced. The length a and width b of the Ligament correspond to the length L of the PKMM side, showing that only one variable is independent. For this work, the Ligament width b will be the primary focus of discussion. At the same time, there is also a geometric correspondence between the angle α and the height h. For thin layer structures, the thickness d always behaves as an insensitive parameter. Therefore, the core of the parameter design of PKMM structure lies in the regulation of Ligament width b and height h.

The width b of Ligament is widened, thereby enhancing the acquisition accuracy of structural buckling deformations. Concurrently, this design enlarges the effective sensing area. Consequently, the transformation from buckling deformations to electrical signals is significantly enhanced. The height h of the PKMM structure exhibits dynamic change during 3D deformation. The size of h only influences the initial height of the structure and the maximum displacement sensing range. Since a larger initial height encompasses the deformation range of a smaller height, conducting comparative experiments on initial height becomes irrelevant. Following the thorough examination of the available evidence, it can be concluded that parameter b represents the primary area of focus for optimisation. Therefore, a scheme with three gradients based on the parameter b is systematically designed. The purpose of this scheme is to elucidate the influence of parameter b on performance metrics used to quantify sensing (Specific parameters in Table S2).

2.2. Mechanical property characterization

The PKMM structure demonstrates remarkable stretchability and

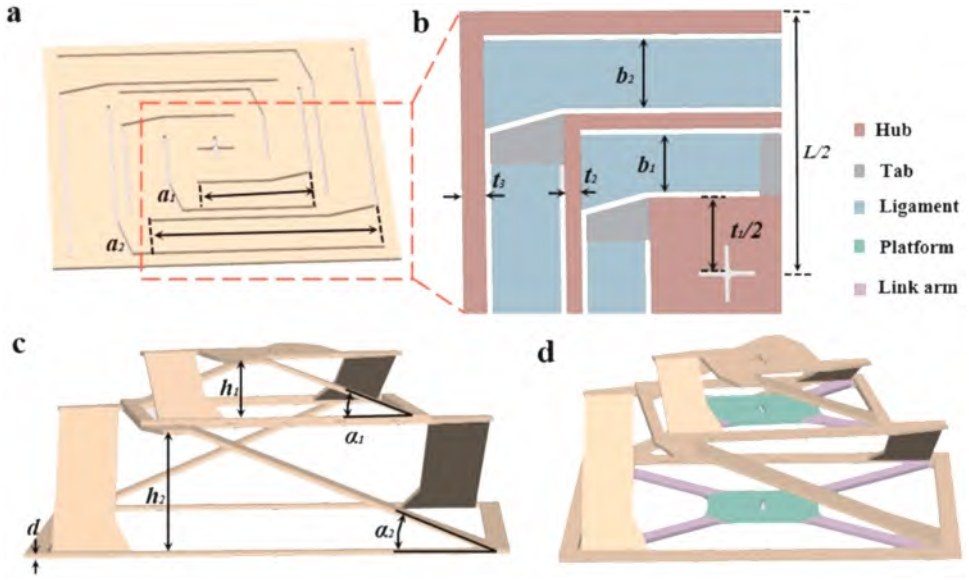

Fig. 1. Schematic diagram of the 2D plane and 3D state of the PKMM structure: (a) planar state. (b) component segmentation. (c) 3D state, and (d) assembled 3D state with integrated components.

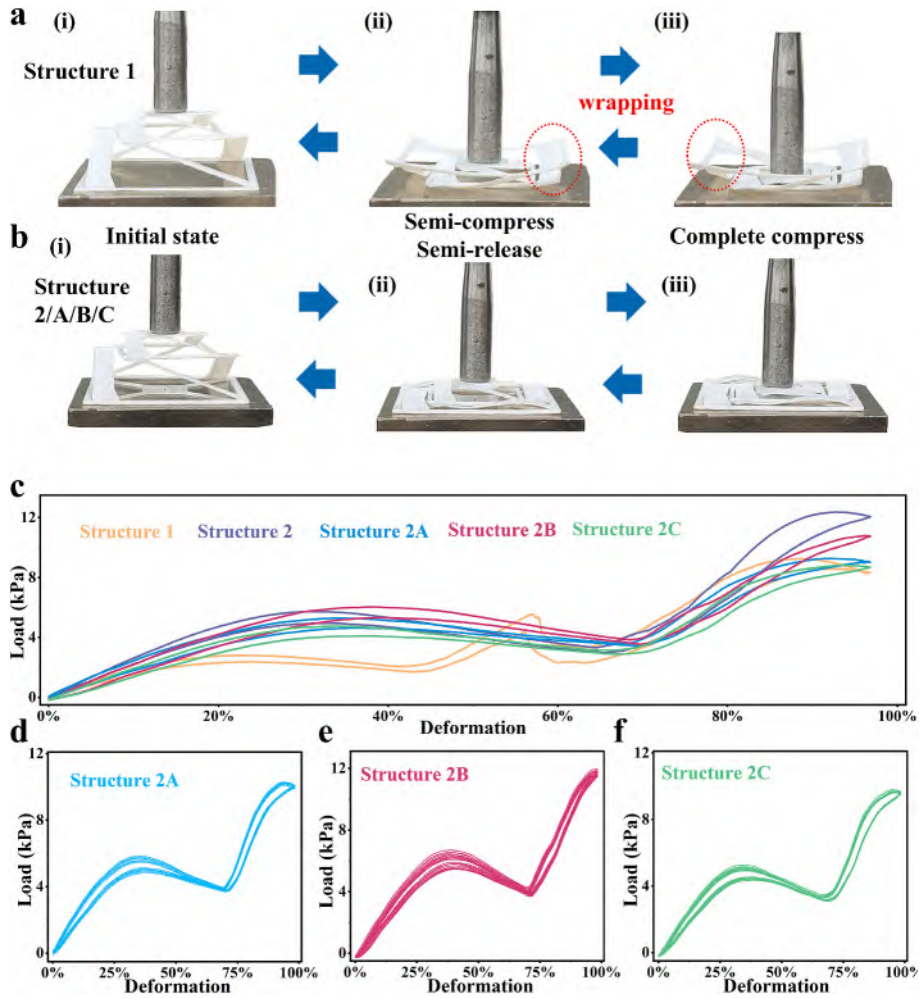

Fig. 2. Deformation behaviour of (a)Structure 1 and (b) Structure 2 under compression. (c) Mechanical response. (d, e, f) Cyclic stability performance of PKMM structures (Structure 2 A, 2B, and 2C).

surface conformability [8,34,39]. However, there are still some research gaps in applied research on the mechanical properties of PKMM 3D state. The fabrication of a PKMM sheet is achieved through the utilisation of 4D printed technology. The sheet can be programmed to undergo an unfolding process into an upright structure when the heating temperature exceeds 70 °C. The resultant upright 3D structure is designated Structure 1. An investigation is conducted into its mechanical properties, for which quasi-static compression experiments are performed. It has been demonstrated that Structure 1 exerts a warping deformation on Hub 3 when subjected to compressive loading (Fig. 2a (ii) and Movie S1). This deformation is caused by inadequate kinematic constraints and the induction of reactive forces due to the buckling deformation of Ligament 2. The loads are initially borne by Hub 3 through this deformation mechanism. Subsequent to this, Tab 2 undergoes deformation, thereby assuming an additional portion of the load from Hub 3. It should be noted that this additional portion does not exceed the deformation threshold of Ligament 1, a consequence of the warping deformation. Consequently, a sudden peak is observed on the load-deformation curve (Fig. 2c). Ligament 1 begins to buckle once the load reaches its deformation threshold, marking the transition of the structure into the second compression stage. However, the sensor needs to achieve a firm fit and conformal contact with the surface of the object being measured. So we added a Platform and Link arm to Structure 1. This optimization serves two primary functions: it restricts the warping of Hub 3, and it provides a foundation for the TENG material. And this structure is designated Structure 2.

Further, we perform quasi-static compression tests on Structure 2 as well. Analysing the load-deformation curve of Structure 2 (Fig. 2c), the process can be divided into three different stages. In the initial compression stage (deformation 0–34%), the structure demonstrates a low stiffness characteristic. In the subsequent second compression stage (deformation 34–70%), the structure exhibits negative stiffness properties. In the third compression stage (deformation 70–98%), the PKMM structure undergoes the second stage of deformation and returns to a low stiffness property. Moreover, the lower layer is twice as high as the upper layer in the configuration of a two-layer PKMM. Semi-compress /semi-release (Fig. 2b(ii)) therefore, corresponds to 70% deformation along the curve. The fully compressed state (Fig. 2b(iii)) corresponds to the deformation of 98% on the curve. The improved mechanical response not only ensures the stability of the structure but also eliminates the load peak of Structure 1. At the same time, the negative stiffness property and high sensitivity property to the external force of the PKMM structure are preserved. It is beneficial to realize accurate corresponding positioning of displacement sensing and provides an ideal structural basis for practical sensing applications.

Following the implementation of the b-based structure optimisation scheme, the PKMM structure with gradient growth is conceptualized for three distinct Ligament widths b (Specific parameters in Table S2). Validated optimization of Structure 2 relative to Structure 1 informed subsequent design enhancements. We integrated intermediate-layer Platforms and Link arms by leveraging the bilayer PKMM. The structures are then designated as Structure 2A, 2B, and 2C, according to the value of Ligament widths b in sequential order. Mechanical properties of these PKMM structures are tested by quasi-static compression experiments. Structure 2B and Structure 2 have identical structural parameters in terms of design. Structure 2B has a dual-platform design, while Structure 2 has a single-platform design. And compression tests show that both structures exhibit indistinguishable deformation after loading. At the same time, Structure 2A, 2B, and 2C designed with different b values , also exhibit similar mechanical response properties during compression (Fig. 2c). These deformation patterns demonstrate minimal functional impact from the intermediate Platform's constraint mechanism. Furthermore, subtly different b exhibits negligible alterations in the global mechanical properties of the structural system. It is confirmed that the design strategy of widening the b mainly plays a role in improving the sensing performance rather than changing the mechanical properties.

In this work, cyclic compression tests are conducted on Structure 2A, 2B, and 2C to assess the reliability and stability of the structures. The load-deformation curves demonstrated remarkable consistency over ten cycles of loading. This outstanding cycling stability affirms the reliability and reusability of the PKMM structure as a displacement sensor. These findings offer a robust experimental foundation for ensuring its long-term stability in real-world engineering applications.

2.3. Electrical property characterization

The output signal of the TENG sensor is focused on the moment of contact between the friction layer materials. It can thus be concluded that the primary function of TENG sensing is to reflect the physical properties of the friction layer material at contact pressure. However, the TENG outputs a long blanking signal in the time domain at each cycle in long-distance displacements where the friction layer materials are separated. This has a substantial impact on the effectiveness of TENG real-time pressure sensing. The direct piezoelectric effect of piezoelectric materials is combined to achieve continuous sensing of pressure changes to address the limitation. These results in the creation of a composite sensing mechanism comprising TENG and piezoelectric sensing. The composite sensing mechanism effectively broadens the pressure sensing range while maintaining high accuracy for lower pressures.

The PKMM demonstrates stable motion deformation behaviour under mechanical loading. Consequently, this work employs a specific sensing function partition design tailored to the force distribution and deformation characteristics (Movie S2). Specifically, a piezoelectric material is integrated as a high-pressure sensor on the top of Hub 1, which experiences the primary load. Ligament 1 and Ligament 2 are designed as conformal sensing areas utilizing flexible piezoelectric sensors that are sensitive to deformation due to their notable buckling strain. Additionally, the Platform is conceptualized as a TENG pressure sensor platform by leveraging its periodic contact-separation properties during compression (Supporting Note S3). This partition design adeptly utilizes the mechanical response of the PKMM across various regions, achieving an organic integration of dual-mode sensing functions.

In this work, a two-layer TENG is fabricated using copper film and polytetrafluoroethylene (PTFE) film as the friction layer materials. The friction layer materials are fixed on the Platform of PKMM as shown in Fig. 3a. The same friction layer materials are connected in series with wires to the positive and negative terminals of an electrostatic meter and then tested for electrical properties. In addition to the wire access, the difference in output between single and double electrode TENG is discussed in Supporting Note S4. The flexible piezoelectric materials are fabricated using the polydimethylsiloxane (PDMS) substrate. Then, polyvinylidene fluoride (PVDF) and nano-barium titanate (n-$BaTiO_3$) as piezoelectric particles are uniformly dispersed within this matrix (Supporting Note S2).

COMSOL Multiphysics simulations quantitatively characterize charge transfer and potential field evolution during TENG contact-separation cycling (Supporting Note S4). It is noteworthy that the two sets of TENGs interact sequentially through contact and separation, rather than concurrently. The outcome can be attributed to the hierarchical deformation of the PKMM. Consequently, the output electrical signal exhibits a distinctive stepped superposition characteristic. The output of the TENG sensor reveals comprehensive electrical signatures in Part (i), encompassing voltage (Fig. 3b), current (Fig. 3c), and charge transfer quantity (Fig. 3d). Part (ii) delivers the temporal evolution of waveform morphology during individual compression-release cycles. As illustrated in Part (ii), the key nodes of the cycle are demonstrated: (i) Initial state of compression; (ii) PKMM is semi-compress with one set of TENGs in contact; (iii) PKMM is completely compressed, with both sets of TENGs in contact; (iv) PKMM is semi-release and one set of TENGs is separated; (i') PKMM is completely released and both sets of TENGs are

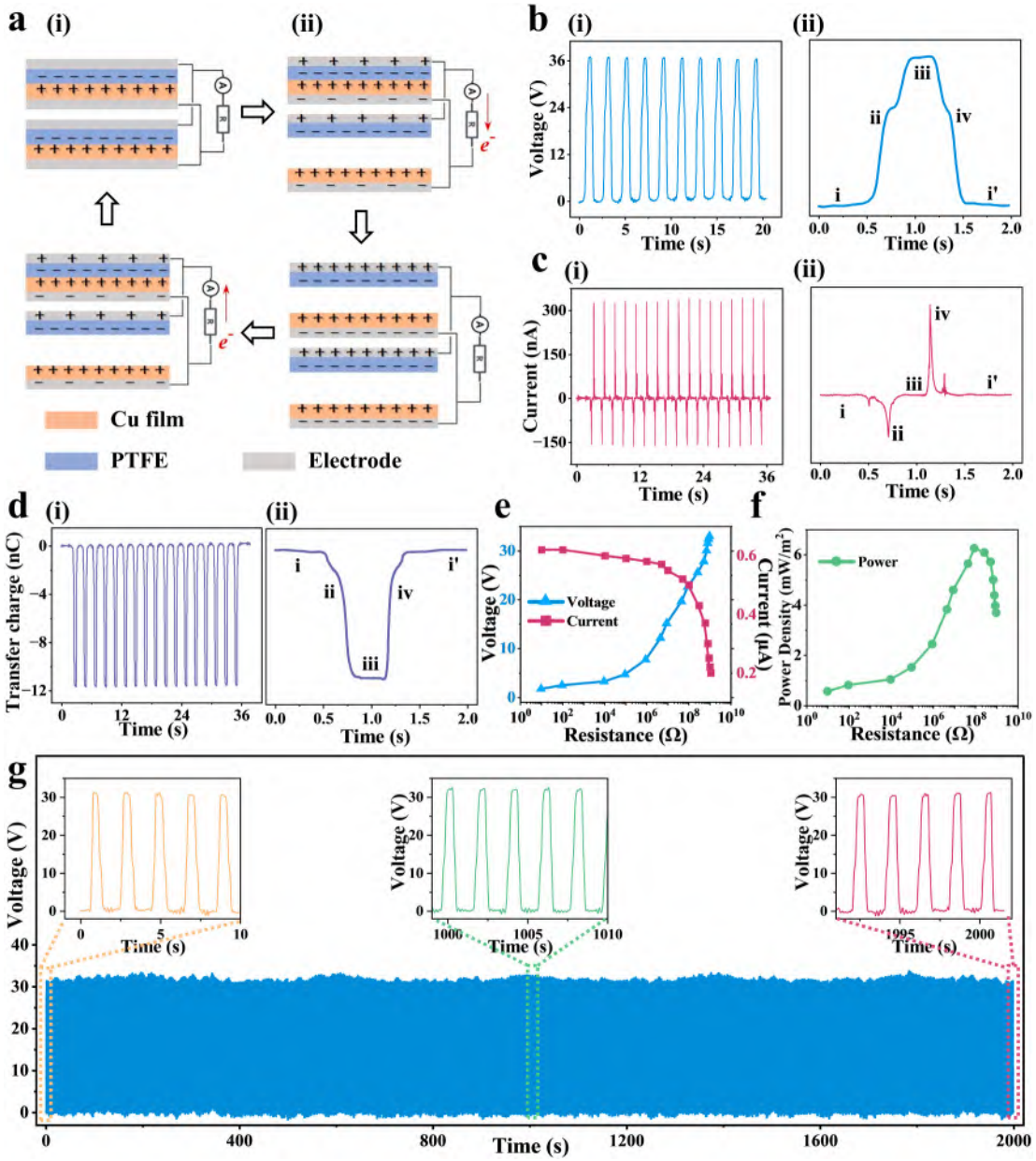

Fig. 3. (a) Schematic illustration of TENG integration within the PKMM structure; Electrical output signal of TENG under mechanical activation: (b) voltage, (c) current, and (d) charge transfer quantity; (ii) Waveform of signals; Electrical performance under load resistance: (e) voltage-current response, (f) power supply density; (g) Durability test of TENG.

separated, returning to the initial state.

When connected to a resistor (Fig. 3e), the output voltage and current of the TENG demonstrate regular fluctuations as the external resistance value increases. At a resistance of 100 MΩ, the system achieves its maximum power density of 6.25 mW/m^2 (Fig. 3f).

$$P = UI \qquad P_s = \frac{P}{A} \qquad A = 2 \times t_1^2 \tag{1}$$

where P_S is the surface power density of the TENG, and the working area of the TENG is the area of Hub 1, which is as large as the material in the experiment. Since two sets of TENG are connected in parallel, the final effective area A needs to be multiplied by 2.

The stability of the TENG has been systematically assessed, as illustrated in Fig. 3g. The output signal demonstrates remarkable consistency, exhibiting only minimal voltage fluctuations even after 1000 consecutive compression cycles. TENG has been demonstrated to facilitate precise and stable sensing functions, whilst also exhibiting exceptional durability and reliability. This provides a robust foundation for the advancement of sensing systems. Furthermore, its contact-separation motion can illuminate numerous bulbs when the PKMM structure is integrated with a TENG connected to LED bulbs (Movie S3).

As illustrated in Fig. 4, the PKMM sensor demonstrates its functionality through the sensing of pressure and displacement. This sensor is based on the composite triboelectric-piezoelectric sensing mechanism. In the description of Figs. 3bcd(ii), each cycle of compression is divided into five stages. These stages will be used as nodes to describe or refer to the different stages of deformation in Figs. 4abc. These figures show the load-displacement curves and time-voltage curves during the compressive deformation of the PKMM structure. Displacement cycle (i) and temporal cycle (ii) exhibit precise synchronization. Their phase correspondence ensures identical horizontal-axis progression. Both parameters map identical compression displacement progression. In the first

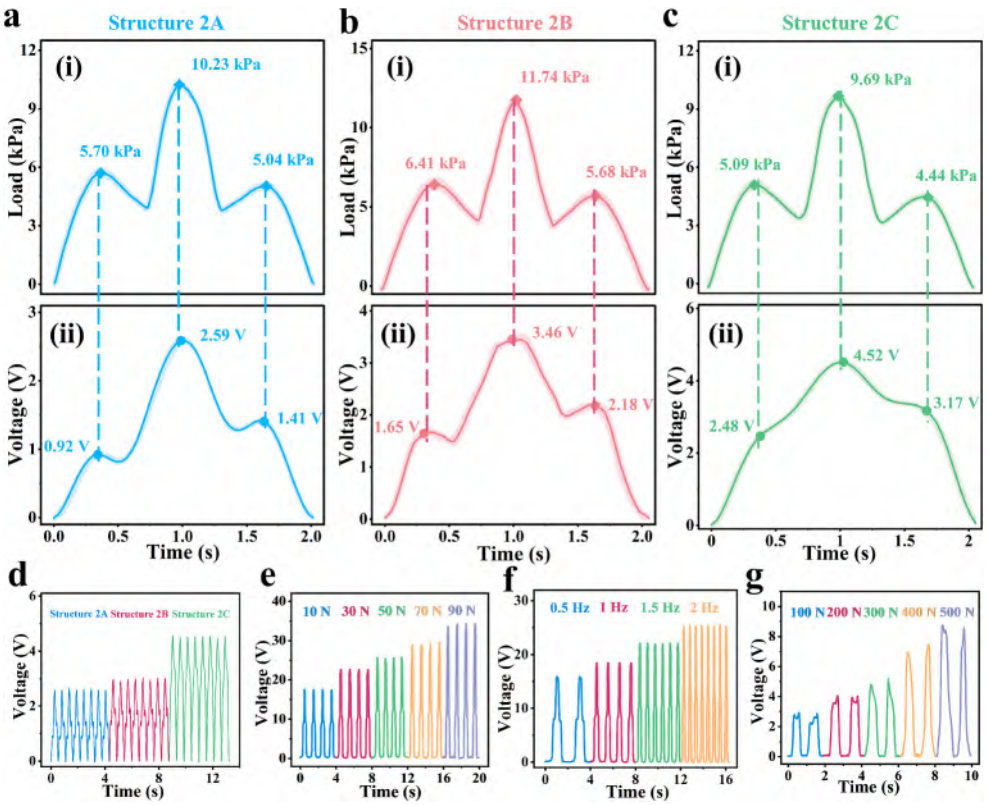

Fig. 4. Demonstrates multimodal sensing characteristics: Displacement sensing accuracy validation during a compression cycle for (a) Structure 2A, (b) 2B, and (c) 2C; (d) Comparative sensing signal amplitudes under identical displacement conditions for Structure 2A, 2B, and 2C, and TENG pressure (e) value sensing, (f) frequency response; (g) Piezoelectric material-based pressure sensing.

and second stage, the PKMM structure is the Ligament buckling deformation. So the sensing signal at this time comes from the buckling deformation of the flexible piezoelectric sensors affixed to the Ligament. In this stage, the displacement in the *Z*-axis direction of the PKMM structure makes the flexible piezoelectric material realize the function of Z-axis displacement sensing. And the TENG gradually starts to contact when the PKMM is about to be completely compressed. The flexible piezoelectric sensors display minimal buckling deformation because the displacement in the Z-axis of the TENG is very small. The voltages and electric field strengths produced by this sensor are significantly lower than those of TENG outputs. Consequently, piezoelectric contributions exert negligible interference on TENG signal integrity. Flexible piezoelectric materials are capable of generating electric fields through the direct piezoelectric effect. The direct piezoelectric effect is contingent upon the mechanical load or strain that occurs in the flexible piezoelectric material. Consequently, the displacement sensing outcomes of flexible piezoelectric sensors are also autonomous from the TENG electric field. Table 1 brings together the mechanical properties of Structure 2A, 2B, and 2C, with intuitive data on sensing signals. The phase distinction of the output signals is used as a key node for comparison between different width *b* and is highlighted in Fig. 4abc.

PKMM structure achieves accurate recording of the overall deformation by integrating flexible piezoelectric sensors. The reliability of the displacement sensing function is fully verified through such a corresponding relationship. The increase in the *b* leads to an expansion of the Ligament area and improvements in the coverage of the flexible piezoelectric material (Fig. 4d). It is concluded that Structure 2C exhibits the best displacement sensing performance, with a sensitivity of 150 mV/mm.

$$S_D = \frac{\Delta U}{\Delta d} \qquad \Delta d = h_1 + h_2 \tag{2}$$

where S_D is the displacement sensing sensitivity and Δd is the displacement distance in sensing.

The experimental results indicate a strong correlation between the output of the TENG and the applied pressure. As shown in Fig. 4e, when the pressure increases from 10 N to 90 N, the output voltage of the TENG rises from 18 V to 32 V, yielding a sensing sensitivity of 315 mV/kPa.

$$S_T = \frac{\Delta U_T}{A} \tag{3}$$

where S_T is the pressure sensing sensitivity of TENG, ΔU_T is the voltage change of TENG, and A is the same as Eq. (1).

TENG sensors precisely monitor pressure frequency variations (Fig. 4f). These experimental observations align with established TENG sensing principles. Consequently, TENG technology demonstrates dual-

Table 1
Mechanical and sensing properties of Structure 2A, 2B, and 2C.

Structure	Width *b*/mm	Semi-compress		Complete compress		Semi-release	
		Load/kPa	Voltage/V	Load/kPa	Voltage/V	Load/kPa	Voltage/V
2A	9	5.7	0.92	10.23	2.59	5.04	1.41
2B	11	6.41	1.65	11.74	3.46	5.68	2.18
2C	13	5.09	2.48	9.69	4.52	4.44	3.17

parameter sensing capability for both load pressure magnitude and action frequency. The TENG friction layer materials are in closer contact with each other when the PKMM structure is subjected to increased compressive loads. This results in a larger contact area of the friction layer materials. So, more electronic exchanges are occurring between the materials with a corresponding increase in the sensing signal. And when a larger compressive load is applied, the PKMM structure no longer changes. At this point, as shown in Fig. 4g, the flexible piezoelectric sensor on the Platform assumes the function of sensing a larger range of pressure.

As for the piezoelectric sensing test (Fig. 4g), the output increases nearly linearly from 2.5 V to 9 V when the pressure increases from 100 N to 500 N. Its pressure sensing sensitivity reaches 14.625 mV/kPa (different from Eq. (2), where *A* only represents the area of a single Hub 1, without multiplying by 2). Its measuring range is significantly expanded, although the sensitivity is lower than that of TENG pressure sensing. Although both the TENG and the flexible piezoelectric sensor are implementing the pressure sensing function at this stage. However, TENGs are pulse-type signals, which mainly generate signals at the moment of contact and separation, and are more accurate for pressure sensing. Piezoelectric materials, on the other hand, are continuous voltage outputs and increase the pressure range significantly. These two sensing signals are not only differentiated in time continuity, but the output voltage magnitude is also significantly different by a factor of several. On this basis, we are able to clearly distinguish whether the sensed signals originate from TENG or flexible piezoelectric materials.

2.4. Shape-morphing and application of PKMM-based sensors

The reconfigurability of the PKMM structure allows for a variety of capabilities, including surface conformity in the 2D state and multistage upright in the 3D state. The PKMM structure can be deformed and reconstructed by raising the temperature above 70 °C, which is the glass transition temperature of the SMP. When heated above 70 °C, the PKMM structure can be programmed to deform into a surface with a specific curvature and is fixed upon cooling. Following a process of reheating, the PKMM structure is restored to its initial state by the SME, with a deformation recovery rate of almost 100%. As shown in Fig. 5a, the same PKMM sheet is deformed and recovered multiple times, exhibiting conformality to a wide range of curvature surfaces. These targeted surfaces comprise three characteristic geometries: (i) cylindrical surfaces exemplified by arms or cups (Fig. 5a(i)); (ii) paraboloids of rotation observed in disk edges (Fig. 5a(ii)); (iii) spherical surfaces representative of helmets and knee pads (Fig. 5a(iii)). The PKMM structure can not only fit a variety of Gaussian curvature surfaces in the 2D state, but also can be configured into multi-level 3D states.

The PKMM can be controlled to present multiple intermediate states in the process of 3D morphology transformation (Fig. 5b). Specifically, part upfold and complete reconfiguration can be obtained by lifting the Hub 1(Fig. 5b(ii), (iii)). And a similar image transformation can be achieved by pushing down (Fig. 5b(iv), (v)). It is observed that the PKMM undergoes relative rotation between platforms when unfolded upright. Chiral symmetric PKMM structures are fabricated to counteract the rotation. The employment of black and white SMP consumables serves to differentiate the structures, thus facilitating the desired effect. Subsequently, these PKMM structures are arranged and combined in the *Z*-axis direction, as illustrated in Fig. 5c. We found that the combined PKMM structures have more diverse deformation states. It has been demonstrated that the arranged structure exhibits markedly divergent deformations in response to pressures from the centre, edge, and corner. Furthermore, it has been observed to generate specific deformation responses to compression in different directions (Movie S4). It is observed

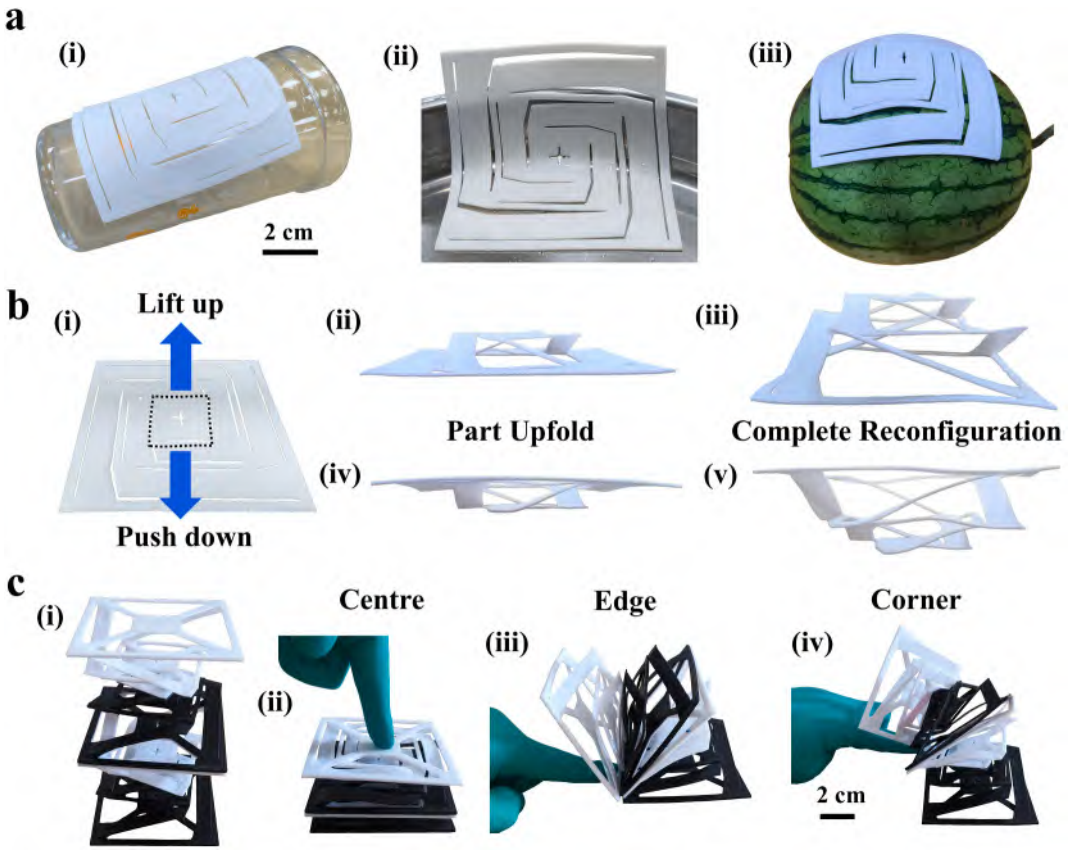

Fig. 5. (a) Conformal representation of plane states of PKMM structure for different surfaces; (b) Different states of PKMM structure under tension or pressure; (c) Multi-directional deformation after axial array.

that the Ligaments in the four directions of the front, back, left, and right of each PKMM structure exhibited different buckling deformations. We can combine flexible piezoelectric sensors to collect and convert these different deformations into voltage signals. Then the output signals of each group of flexible piezoelectric sensors can be analysed to know the deformation of each group of Ligaments of the PKMM structure. Further, the combined bending angle and direction of the PKMM can be deduced. Ultimately, the identification and sensing of multiple complex deformations can be realised.

As illustrated in Fig. 6, this work is illustrated in practice and is based on the structural deformation shown in Fig. 5. Firstly, the PKMM 2D state is fabricated into the shape of a curved elbow surface. Then, the edges of the sheet are attached to the skin near the elbow joint when the arm is straightened. When the elbow is bent to a certain angle respectively, the stretching of the skin causes the elbow joint to push the PKMM out of a certain out-of-plane deformation. As shown in Fig. 6a, the unfolding process of the PKMM 2D state is identical to the piezoelectric sensing effect caused by the compression process of its 3D state. Consequently, the elbow bending angle can be determined from the voltage output signal of the flexible piezoelectric strain sensor. The elbow bending angle and the *Z*-axis displacement caused by the unfolding of the PKMM structure can be correlated to enable real-time monitoring of the elbow bending condition. The deformation recovery of the PKMM structure is close to 100%, while the buckling strain sensing of the flexible piezoelectric material is entirely dependent on the modulus of the structure. Therefore, the PKMM sensor can maintain stable sensitivity and real-time sensing.

As posited in Fig. 5c, this work aims to ascertain whether a PKMM possesses the capacity to discern deformations occurring in various directions and angular orientations. The flexible piezoelectric material is integrated on the surface of the Ligament of the PKMM structure to form a buckling strain sensor. As shown in the built-in inset of Fig. 6b, we label nine points of force concentration on Hub 1 of the PKMM. Subsequently, rigorous testing is undergone by the sensing of the buckling deformation of the Ligament above the PKMM. This involves the application of a concentrated force at each of the nine points (Movie S5). The results demonstrate that the buckling strains induced by the application of concentrated forces at varying points can be recognised and sensed as output. Moreover, each PKMM in the axial array and the flexible piezoelectric sensors on each Ligament operate independently (Movie S6). It can thus be concluded that the recognition of multi-dimensional complex deformations can be achieved after the axial array of PKMM structures. This axial-arrayed PKMM sensor overcomes the limitations of traditional one-dimensional linear sensing. The objective of this work is to demonstrate the capacity for precise monitoring of multi-dimensional motion. This breakthrough provides a new technical approach for developing high-performance multi-dimensional motion sensors.

Finally, we design bases to inlay PKMM structures and form them into 3 × 3 arrays, connecting the bases with a centre-cutting Kirigami pattern with excellent tensile properties [7,39–41]. It is necessary to ensure that the deformations between these units do not influence each

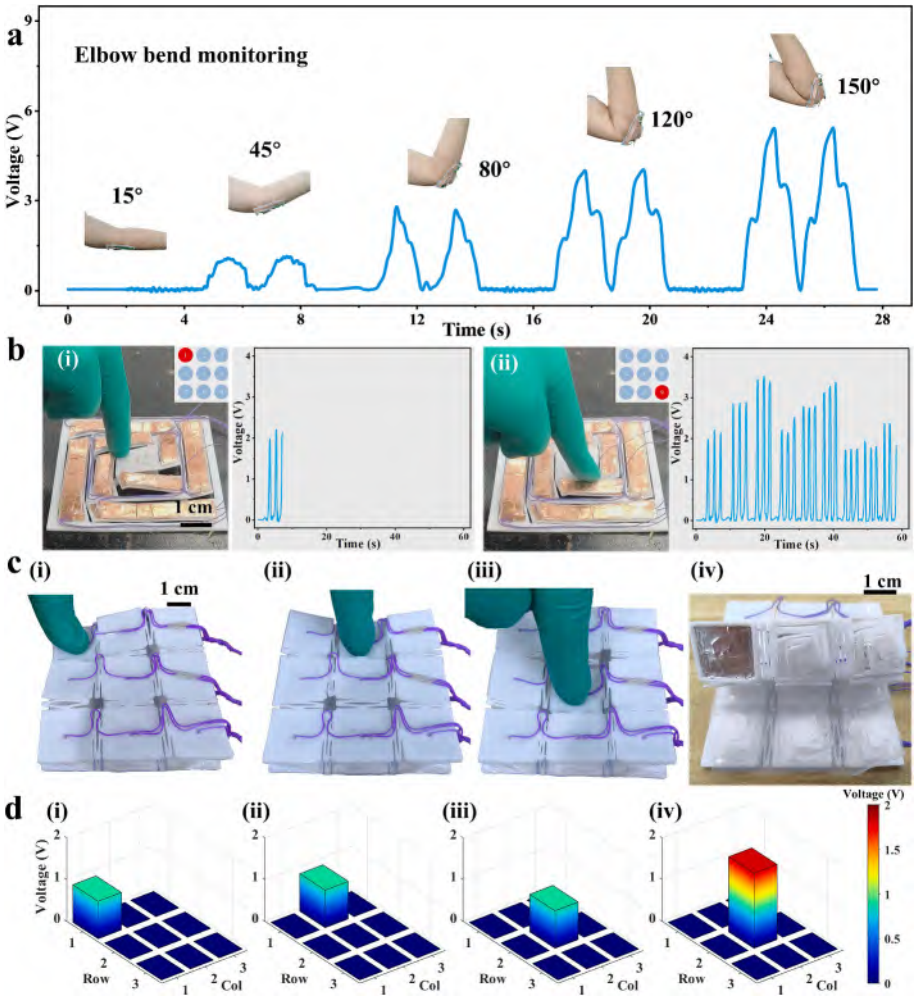

Fig. 6. (a) Planar-state PKMM structure for real-time elbow joint motion monitoring; (b) 3D-state PKMM structure monitoring of the force at different concentrated force points; Island-bridge array exhibiting (c) multipoint pressure response and (d) load intensity detection under localized stimuli.

other to prevent crosstalk between neighbouring sensing units. This objective can be realised by reducing the modulus of the centre-cutting Kirigami. Mitigating crosstalk between adjacent sensing units requires a reduction in the modulus of the centre-cutting Kirigami. This mechanical optimisation stops the actuation of one array unit from propagating to neighbouring elements during compressive loading. On the one hand, reducing the width of the ribbon of centre-cutting Kirigami can effectively reduce the modulus and enhance its tensile properties. On the other hand, we chose to print the base in TPU 90A with a lower modulus. And then we still used SMP to print the PKMM in an isometrically reduced planar state (every sheet with a size of about 2 × 2 cm). The PKMM structure is then programmed to be fixed in an upright unfolded state above 70 °C. As shown in Fig. 6c(iv), the electrodes are fixed to the bases while the two array bases inlaid with nine unfolded PKMM structures are separated by PTFE and act as a friction layer. Thus, the 3 × 3 island-bridge array of TENG multi-point sensors is designed to accomplish sensing detection of pressure distribution. The sensing results are shown in Fig. 6d, where (i), (ii), and (iii) exhibit the sensing of pressure distribution from corners, edges, and centres, respectively, and (iv) feedback of the response to larger pressure loads.

The design of the island-bridge array with multiple units has significant advantages. Firstly, its excellent stretchability and conformability enable it to adapt to complex surfaces. Secondly, its modular design facilitates the expansion of multiple functions. Moreover, this array scheme proposed in this work can be extended by further deep refinement. The method of fabrication for 2D structures has reached a sufficient level of maturity to reduce the size of PKMM structures. The arrangement of the sampling points of the array can be accommodated in a more dense configuration. Moreover, the integration of TENG in this process remains unaffected by dimensional variations. In this way, the accuracy obtained with island-bridge arrays can be greatly improved, and the number of sensing and monitoring pixels increased significantly. For example, it can be integrated into a helmet or knee pad to monitor impact and load intensity during exercise, providing a quantitative basis for injury assessment and treatment. Alternatively, direct integration onto insole surfaces enables precise mapping of plantar pressure distribution during gait cycles. This methodology generates critical datasets for advancing locomotion biomechanics research. This multifunctional integrated design opens up a new technical path for the development of a new generation of smart wearable devices.

3. Conclusion

In this work, we successfully design a smart sensor system with a 4D printed PKMM structure. A composite sensing mechanism has been innovatively applied in the sensor system incorporating triboelectric and piezoelectric technologies. The regulatory law of the Ligament width b on the sensing performance is revealed. Subsequently, the rationality of the widened Ligament design under consideration is verified in this work. The sensor system delineated in this work exhibits superior comprehensive performance, with the TENG sensor attaining a high sensitivity of 315 mV/kPa in pressure sensing. The combination with the piezoelectric sensors has two main effects. Firstly, it expands the axial pressure sensing range. Secondly, it complements the discontinuity of TENG sensing. Concurrently, the flexible piezoelectric sensor can convert the buckling strain of the Ligament into precise localisation of the displacement. PKMM has been shown to deform hierarchically and conform to surfaces through reconfiguration, and has been used to monitor joint motion. The independent operation of PKMM Ligaments facilitates the identification of multi-dimensional complex deformations. The configuration of the island-bridge array serves to further substantiate the capacity of PKMM for multi-point load distribution detection. This work provides novel concepts for the design and application of self-powered flexible sensors, which have significant applications in the domains of wearable medicine and intelligent robotics.

Supplementary data to this article can be found online at https://doi.org/10.1016/j.cej.2025.165392.

CRediT authorship contribution statement

Song Liu: Writing – original draft, Validation, Conceptualization. **Zhaoxuan Niu:** Writing – review & editing, Visualization, Formal analysis. **Wei Zhao:** Writing – review & editing, Resources, Methodology, Formal analysis. **Chengjun Zeng:** Methodology, Conceptualization. **Yanju Liu:** Supervision, Project administration, Funding acquisition. **Jinsong Leng:** Supervision, Project administration, Funding acquisition.

Declaration of competing interest

The authors declare that they have no known competing financial interests or personal relationships that could have appeared to influence the work reported in this paper.

Acknowledgments

This work is supported by the National Key Research and Development Program of China (2022YFB3805700, 2024YFB4710205), National Natural Science Foundation of China (Grant No. 92271206, 12472147, U23A20412, 12402160), the Research Fund of State Key Laboratory of Mechanics and Control for Aerospace Structures (Nanjing University of Aeronautics and astronautics) (Grant No. MCAS-E-0224G02), and Young Elite Scientists Sponsorship Program by CAST (Grant No. 2023QNRC001), Heilongjiang Provincial Natural Science Foundation of China 2022ZX02C25.

Data availability

Data will be made available on request.

References

[1] X. Li, W. Peng, W. Wu, J. Xiong, Y. Lu, Auxetic mechanical metamaterials: from soft to stiff, Int. J. Extreme Manuf. 5 (2023) 042003, https://doi.org/10.1088/2631-7990/ace668.
[2] Wei Zhao, Nan Li, Xu Liu, Liwu Liu, Chengbin Yue, Chengjun Zeng, Yanju Liu, 4D printed shape memory metamaterials with sensing capability derived from the origami concept, Nano Energy 115 (2023) 108697, https://doi.org/10.1016/j.nanoen.2023.108697.
[3] N.I. Zheludev, The road ahead for metamaterials, Science 328 (2010) 582–583, https://doi.org/10.1126/science.1186756.
[4] P. Jiao, J. Mueller, J.R. Raney, X. Zheng, A.H. Alavi, Mechanical metamaterials and beyond, Nat. Commun. 14 (2023) 6004, https://doi.org/10.1038/s41467-023-41679-8.
[5] L. Wu, D. Pasini, Zero modes activation to reconcile floppiness, rigidity, and multistability into an all-in-one class of reprogrammable metamaterials, Nat. Commun. 15 (2024) 3087, https://doi.org/10.1038/s41467-024-47180-0.
[6] S. Babaee, Y. Shi, S. Abbasalizadeh, S. Tamang, K. Hess, J.E. Collins, K. Ishida, A. Lopes, M. Williams, M. Albaghdadi, A.M. Hayward, G. Traverso, Kirigami-inspired stents for sustained local delivery of therapeutics, Nat. Mater. 20 (2021) 1085–1092, https://doi.org/10.1038/s41563-021-01031-1.
[7] M.K. Blees, A.W. Barnard, P.A. Rose, S.P. Roberts, K.L. McGill, P.Y. Huang, A. R. Ruyack, J.W. Kevek, B. Kobrin, D.A. Muller, P.L. McEuen, Graphene kirigami, Nature 524 (2015) 204–207, https://doi.org/10.1038/nature14588.
[8] X. Li, P. Zhu, S. Zhang, X. Wang, X. Luo, Z. Leng, H. Zhou, Z. Pan, Y. Mao, A self-supporting, conductor-exposing, stretchable, ultrathin, and recyclable kirigami-structured liquid metal paper for multifunctional e-skin, ACS Nano 16 (2022) 5909–5919, https://doi.org/10.1021/acsnano.1c11096.
[9] A.M. Barboza, L.C.R. Aliaga, D. Faria, I.N. Bastos, Bilayer graphene kirigami, Carbon Trends 9 (2022) 100227, https://doi.org/10.1016/j.cartre.2022.100227.
[10] X. Shi, Y. Wei, B. Tang, Y. Li, L. Lv, S. Lin, S. Luo, T. Wang, S. Tan, Q. Sun, X. Wang, X. Zheng, Y. Guo, F. Liang, W. Huang, H.-D. Yu, A Kirigami-driven stretchable paper-based Hydrovoltaic electricity generator, Adv. Funct. Mater. (2025), https://doi.org/10.1002/adfm.202419753, 2419753.
[11] J. Tao, H. Khosravi, V. Deshpande, S. Li, Engineering by cuts: how Kirigami principle enables unique mechanical properties and functionalities, Adv. Sci. 10 (2023), https://doi.org/10.1002/advs.202204733, 2204733.
[12] Z. Ren, S. Deng, J. Shao, Y. Si, C. Zhou, J. Luo, T. Wang, J. Li, J. Li, H. Liu, X. Qi, P. Wang, A. Yin, L. Wu, S. Yu, Y. Zhu, J. Chen, S. Das, J. Wei, Z. Chen, Ultrahigh-power-density flexible piezoelectric energy harvester based on freestanding

ferroelectric oxide thin films, Nat. Commun. 16 (2025) 3192, https://doi.org/10.1038/s41467-025-58386-1.
[13] C. Tang, Z. Liu, L. Li, Mechanical sensors for cardiovascular monitoring: from battery-powered to self-powered, Biosensors 12 (2022) 651, https://doi.org/10.3390/bios12080651.
[14] Z. Nie, J.W. Kwak, M. Han, J.A. Rogers, Mechanically active materials and devices for bio-interfaced pressure sensors—a review, Adv. Mater. 36 (2024) 2205609, https://doi.org/10.1002/adma.202205609.
[15] P. Basset, S.P. Beeby, C. Bowen, Z.J. Chew, A. Delbani, R.D.I.G. Dharmasena, B. Dudem, F.R. Fan, D. Galayko, H. Guo, J. Hao, Y. Hou, C. Hu, Q. Jing, Y.H. Jung, S.K. Karan, S. Kar-Narayan, M. Kim, S.-W. Kim, Y. Kuang, K.J. Lee, J. Li, Z. Li, Y. Long, S. Priya, X. Pu, T. Ruan, S.R.P. Silva, H.S. Wang, K. Wang, X. Wang, Z. L. Wang, W. Wu, W. Xu, H. Zhang, Y. Zhang, M. Zhu, Roadmap on nanogenerators and piezotronics, APL Mater. 10 (2022) 109201, https://doi.org/10.1063/5.0085850.
[16] J. Li, J. Cai, J. Yu, Z. Li, B. Ding, The rising of Fiber constructed piezo/triboelectric Nanogenerators: from material selections, fabrication techniques to emerging applications, Adv. Funct. Mater. 33 (2023) 2303249, https://doi.org/10.1002/adfm.202303249.
[17] X. Lv, Y. Liu, J. Yu, Z. Li, B. Ding, Smart fibers for self-powered electronic skins, Adv. Fiber Mater. 5 (2023) 401–428, https://doi.org/10.1007/s42765-022-00236-6.
[18] K. Xia, M. Yu, Highly robust and efficient metal-free water cup solid–liquid triboelectric nanogenerator for water wave energy harvesting and ethanol detection, Chem. Eng. J. 503 (2025) 157938, https://doi.org/10.1016/j.cej.2024.157938.
[19] W.-G. Kim, D.-W. Kim, I.-W. Tcho, J.-K. Kim, M.-S. Kim, Y.-K. Choi, Triboelectric Nanogenerator: structure, mechanism, and applications, ACS Nano 15 (2021) 258–287, https://doi.org/10.1021/acsnano.0c09803.
[20] J. Luo, Z. Wang, L. Xu, A.C. Wang, K. Han, T. Jiang, Q. Lai, Y. Bai, W. Tang, F. R. Fan, Z.L. Wang, Flexible and durable wood-based triboelectric nanogenerators for self-powered sensing in athletic big data analytics, Nat. Commun. 10 (2019) 5147, https://doi.org/10.1038/s41467-019-13166-6.
[21] J. Fu, K. Xia, Z. Xu, Double helix triboelectric nanogenerator for self-powered weight sensors, Sens. Actuators Phys. 323 (2021) 112650, https://doi.org/10.1016/j.sna.2021.112650.
[22] Z. Zhu, H. Zhang, K. Xia, Z. Xu, Pencil-on-paper strain sensor for flexible vertical interconnection, Microsyst. Technol. 24 (2018) 3499–3502, https://doi.org/10.1007/s00542-018-3759-8.
[23] Z. Xu, C. Zhang, F. Wang, J. Yu, G. Yang, R.A. Surmenev, Z. Li, B. Ding, Smart textiles for personalized sports and healthcare, Nano-Micro Lett. 17 (2025) 232, https://doi.org/10.1007/s40820-025-01749-6.
[24] H. Liu, D. Li, H. Chu, Y. Ding, Z. Fu, X. Yao, J. Zhu, J. Yang, R. Liu, T. Xu, S. Fu, Y. Liu, Y. Han, Y. Wang, Y. Zhao, X. Cui, Y. Tian, Ultra-stretchable triboelectric touch pad with sandpaper micro-surfaces for transformer-assisted gesture recognition, Nano Energy 130 (2024) 110110, https://doi.org/10.1016/j.nanoen.2024.110110.
[25] K. Xia, Z. Zhu, H. Zhang, C. Du, R. Wang, Z. Xu, High output compound triboelectric Nanogenerator based on paper for self-powered height sensing system, IEEE Trans. Nanotechnol. 17 (2018) 1217–1223, https://doi.org/10.1109/TNANO.2018.2869934.
[26] K. Xia, Z. Xu, Z. Zhu, H. Zhang, Y. Nie, Cost-effective copper–nickel-based triboelectric nanogenerator for corrosion-resistant and high-output self-powered wearable electronic systems, Nanomaterials 9 (2019) 700, https://doi.org/10.3390/nano9050700.
[27] H. Ouyang, Z. Liu, N. Li, B. Shi, Y. Zou, F. Xie, Y. Ma, Z. Li, H. Li, Q. Zheng, X. Qu, Y. Fan, Z.L. Wang, H. Zhang, Z. Li, Symbiotic cardiac pacemaker, Nat. Commun. 10 (2019) 1821, https://doi.org/10.1038/s41467-019-09851-1.
[28] K. Xia, D. Wu, J. Fu, N.A. Hoque, Y. Ye, Z. Xu, Tunable output performance of triboelectric nanogenerator based on alginate metal complex for sustainable operation of intelligent keyboard sensing system, Nano Energy 78 (2020) 105263, https://doi.org/10.1016/j.nanoen.2020.105263.
[29] S. Xu, W. Nie, J. Sun, P. Sun, H. Jia, X. Zheng, Y. Sun, Z. Xu, L. Liu, Multi-mode and durable fiber triboelectric nanogenerator for power and sensor enabled by Hookean vascular stent structure, Chem. Eng. J. 472 (2023) 145088, https://doi.org/10.1016/j.cej.2023.145088.
[30] C. Wu, X. Wang, L. Lin, H. Guo, Z.L. Wang, Paper-based triboelectric Nanogenerators made of stretchable interlocking Kirigami patterns, ACS Nano 10 (2016) 4652–4659, https://doi.org/10.1021/acsnano.6b00949.
[31] Y. Miyamoto, Rotational erection system (res): origami extended with cuts, Origami^{6} (2015) 537–544. doi:https://doi.org/10.1090/mbk/095.2/16.
[32] Q. Zhang, N. Pan, S. Liu, J. Feng, J. Cai, Self-locking Kirigami surfaces via controlled stretching, Commun. Eng. 3 (2024) 26, https://doi.org/10.1038/s44172-024-00169-5.
[33] X. Li, Y. Gai, M. Sun, Y. Li, S. Xu, Drum tower-inspired kirigami structures for rapid fabrication of multifunctional shape-memory smart devices with complex and rigid 3d geometry in a two-stage photopolymer, Adv. Funct. Mater. 32 (2022), https://doi.org/10.1002/adfm.202205842, 2205842.
[34] L. Hong, H. Zhang, T. Kraus, P. Jiao, Ultra-stretchable kirigami piezo-metamaterials for sensing coupled large deformations, Adv. Sci. 11 (2024), https://doi.org/10.1002/advs.202303674, 2303674.
[35] M. Isobe, K. Okumura, Continuity and discontinuity of kirigami's high-extensibility transition: a statistical-physics viewpoint, Phys. Rev. Res. 1 (2019) 022001, https://doi.org/10.1103/PhysRevResearch.1.022001.
[36] Peng Zhao, Zhaoxuan Niu, Chengjun Zeng, Wei Zhao, Jinsong Leng, Design and functional verification of a flexible wireless spinal cord stimulator with spinal motion monitoring function, Nano Energy 139 (2025) 110895, https://doi.org/10.1016/j.nanoen.2025.110895.
[37] E. Yarali, M.J. Mirzaali, A. Ghalayaniesfahani, A. Accardo, P.J. Diaz-Payno, A. A. Zadpoor, 4D printing for biomedical applications, Adv. Mater. 36 (2024), https://doi.org/10.1002/adma.202402301, 2402301.
[38] Y. Xia, Y. He, F. Zhang, Y. Liu, J. Leng, A review of shape memory polymers and composites: mechanisms, materials, and applications, Adv. Mater. 33 (2021), https://doi.org/10.1002/adma.202000713, 2000713.
[39] K. Meng, X. Xiao, Z. Liu, S. Shen, T. Tat, Z. Wang, C. Lu, W. Ding, X. He, J. Yang, J. Chen, Kirigami-inspired pressure sensors for wearable dynamic cardiovascular monitoring, Adv. Mater. 34 (2022) 2202478, https://doi.org/10.1002/adma.202202478.
[40] Y. Guan, Z. Zhang, Y. Tang, J. Yin, S. Ren, Kirigami-inspired nanoconfined polymer conducting nanosheets with 2000% stretchability, Adv. Mater. 30 (2018) 1706390, https://doi.org/10.1002/adma.201706390.
[41] H. Zhang, J. Wu, D. Fang, Y. Zhang, Hierarchical mechanical metamaterials built with scalable tristable elements for ternary logic operation and amplitude modulation, Sci. Adv. 7 (2021), https://doi.org/10.1126/sciadv.abf1966 eabf1966.